nature communications

Article

https://doi.org/10.1038/s41467-025-60674-9

Organometallic-type reactivity of stable organoboronates for selective (hetero)arene C–H/C-halogen borylation and beyond

Received: 11 January 2025

Accepted: 29 May 2025

Published online: 01 July 2025

Check for updates

Xueting Liu[1], Daojing Li[1], Guoao Li[1], Mengran Wei[1], Shihao Yuan[1], Mo Yang[1], Linke He[1], Shengda Chen[1], Zhenxing Li[1], Liuzhou Gao[2], Guoqiang Wang[1] ✉ & Shuhua Li[1] ✉

Organometallic reagents are essential tools in both academic and industrial laboratories and the polarity separation within the carbon-metal bonds endows them with exceptional reactivities, but also imposes limitations, including air- and moisture-sensitivity, and flammability. Here, we demonstrate that stable and easily accessible benzylic (or allylic) boronate with alkali-metal alkoxide as the activator can act as reactive organometallic reagents. This strategy enables transition metal-free deprotonative C–H borylation of diverse (hetero)arenes. The polar organometallic nature of this process enables predictable and site-selective borylation by targeting the arenes's most acidic C–H bond. This approach can be coupled with Suzuki-Miyaura reaction to produce C–H arylation products. We have also applied this strategy to the dehalogenative borylation of aryl bromides and anionic polymerization of styrenes. Given the unique stability and structural diversity of organoboronates, their organometallic-type reactivities show promise as a powerful alternative to synthetic methodologies that rely on sensitive organometallic reagents.

Organometallic reagents have been a fundamental and indispensable label in both academic and industrial chemical synthesis since their discovery in the early 1900s[1]. The polarity separation existing in the carbon-metal bonds endows them with remarkable nucleophilicity and basicity. After a century of evolution iteration, they have been adapted to a wide range of carbanion-based synthetic transformations like C–H deprotonative metalation, metal-halogen exchange, and anionic polymerization[2–4] (Fig. 1a), providing an alternative to transition metal-catalyzed chemical processes. Their exceptional reactivity also leads to severe limitations, including being highly sensitive to air and moisture, and highly flammable when exposed to air (particularly for organolithiums). Organometallic reagents must be manipulated and stored in strictly dried solvents and inert atmospheres. To overcome these issues, innovations for delivering organolithiums like using deep eutectic solvent[5], organolithium gels[6] and continuous-flow processes[7,8] have been introduced. While these technologies mitigate some sensitivity issues during synthetic operation, organometallic reagents still necessitate stringent air and moisture precautions during both preparation and storage. Therefore, the exploration of versatile and more practical organometallic chemistry schemes remains an active subject.

Organoboronates are widely known as stable organometallic reagents due to the covalent nature of C–B bonds. In the toolbox of synthetic chemists, they are typically used as a carbon coupling unit for the formation of C–C and C–X bonds[9–11] (e.g., Suzuki-Miyaura cross-coupling)[12–14], where boronic ester units act as key leaving groups (Fig. 1b). Although organoboronates have less polarized C–B bonds compared to the celebrated organometallic reagents like organolithium and Grignard reagents[15], it has been reported that several types

[1]State Key Laboratory of Coordination Chemistry, Key Laboratory of Mesoscopic Chemistry of Ministry of Education, School of Chemistry and Chemical Engineering, New Cornerstone Science Laboratory, Nanjing University, Nanjing, P. R. China. [2]School of Chemistry and Chemical Engineering, Yangzhou University, Yangzhou, P. R. China. ✉e-mail: wangguoqiang710@nju.edu.cn; shuhua@nju.edu.cn

https://doi.org/10.1038/s41467-025-60674-9

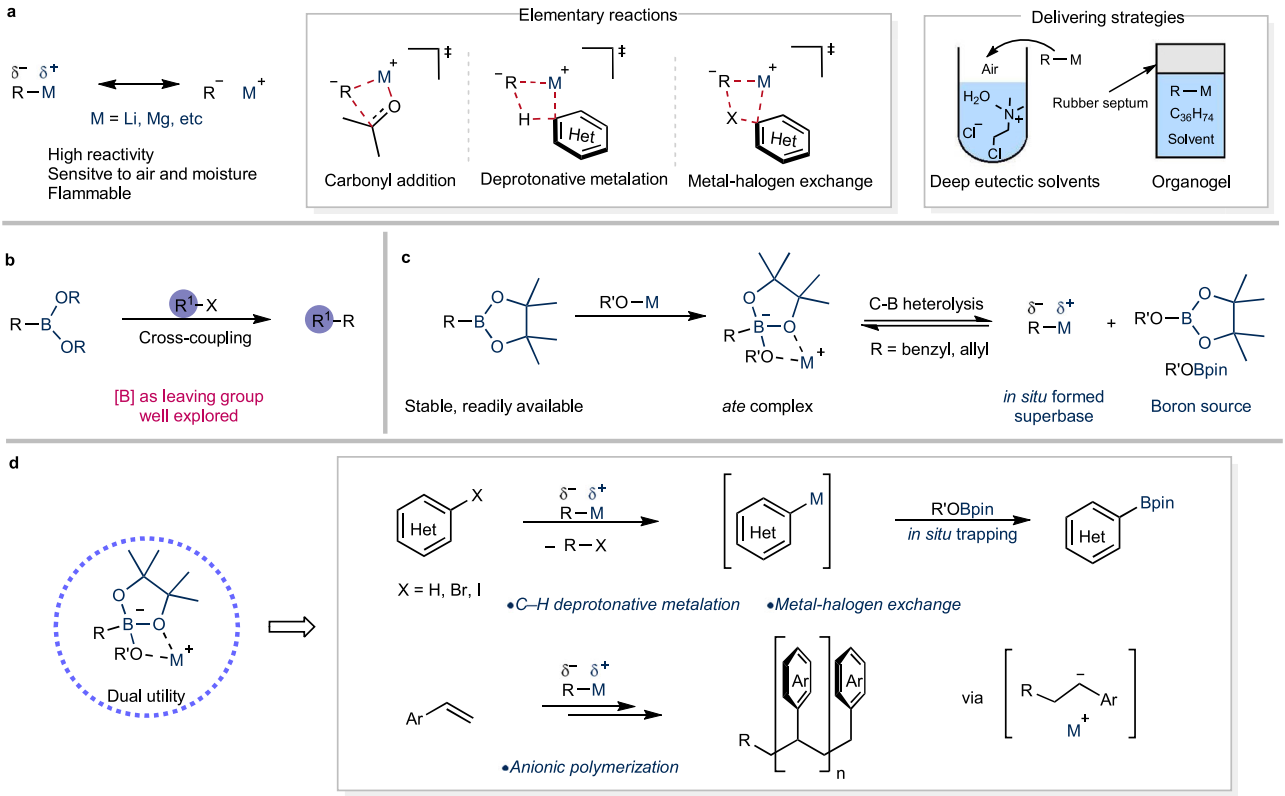

Fig. 1 | Multifaceted reactivity of organometallic reagents. a Representative elementary reactions of polarized organometallic reagents (e.g., organolithium, organomagnesium reagents, etc.) and exemplified strategies for delivering sensitive organometallic reagents. **b** Organoboronates are typically used as a cross-coupling partner for C−C bond constructions with boron unit [B] as a leaving group. **c** In the presence of alkali-metal alkoxides, benzylic (or allylic) boronates might be considered as both superbase precursors and boron sources through the in situ heterolysis of the C−B bond. **d** Outline of the possible transformations using organoboronates/alkali-metal alkoxides combinations as reactive organometallic reagents via deprotonative metalation, metal-halogen exchange or anionic polymerization, in analogy to sensitive organolithiums, organomagnesiums, etc.

of organoboronates (such as benzylic boronates, etc.) could undergo heterolytic cleavage of C−B bonds when associated with alkali-metal alkoxides (ate complex), generating more reactive carbanion species[16]. We therefore envisioned that stable organoboronates could function as a distinct type of highly reactive carbanion precursor (Fig. 1c), capable of replicating the polar reactivity known in classical organometallic reagents. These in situ generated carbanions could therefore be used in similar mechanistic scenarios to those involving superbases (e.g., C−H deprotonative metalation, metal-halogen exchange, etc), substantially expanding the synthetic versatility of organoboronates. More importantly, leveraging their unique stability and widespread availability, the use of these organoboronates as superbase precursors offers a simple, practical, and user-friendly alternative to conventional carbanion-based synthetic methods.

Here, we report the dual utility of benzylic (or allylic) boronates, which can not only replicate the reactivity of highly reactive organometallic reagents but also serve as boron sources (Fig. 1d). The combination of benzylic (or allylic) boronates and alkali-metal alkoxides could in situ afford the related carbanions, and their capacity to deprotonate C−H bonds and undergo metal-halogen exchanges has enabled the development of borylation reactions with broadly available (hetero)arenes and aryl bromides through in situ trapping by the borate ester species. This strategy for in situ generation of organometallic species could also initiate the anionic polymerization of aromatic alkenes[17,18]. In comparison with the synthetic processes based on organometallic reagents[19–21], the advantage of this strategy lies in its stable and easy-to-handle precursors and easy control of reactivity through the flexible selection of different boronates/alkali-metal alkoxide combinations.

Results

Reaction development and mechanistic insight

We initiated our study by screening appropriate boronates as the potential precursors of carbanions (Fig. 2a). Density functional theory (DFT) calculations show that the combinations of benzylic (**1a**–**c**) or allylic (**1d**) boronate/potassium *tert*-butoxide (KO^{t}Bu)[22] are predicted to be kinetically feasible, allowing C−B heterolytic cleavage to generate the related resonance stabilized carbanion intermediates ($\Delta G^{\ddagger}$ = 16.0 ~ 19.5 kcal/mol). The activation of *tert*-butyl borate ^{t}BuBpin (**1e**) with KO^{t}Bu is thermodynamically and kinetically unfavorable ($\Delta G^{\ddagger}$ = 33.5 kcal/mol). To investigate the potential superbase reactivity of these combinations, we chose the deprotonative borylation of N-methylindole **2**, using boronates **1a**–**e** as the boron sources and KO^{t}Bu as a moderate base (Fig. 2b). As expected, reactions of benzylic (or allylic) boronates (**1a**-**1d**) with N-methylindole, excluding ^{t}BuBpin (**1e**), consistently produced C2 borylated indole with moderate to excellent yields (see Supplementary Table 1 for optimization details). It should be noted that the optimal boron source, dimethyl benzylic boronate (**1c**), is readily synthesized through a nickel-catalyzed hydroboration reaction of α-methylstyrene (51% yield, in 50 mmol scale)[23], a significant by-product of the cumene process (over 292,000 tons annually[24]). In addition, these boron compounds are stable to air and moisture. Furthermore, the involvement of a transition-metal-mediated mechanism was excluded by the deliberate introduction of catalytic amounts of several transition metal catalysts, which did not result in any performance enhancement (Supplementary Fig. 4).

Control experiments and NMR analysis were then performed to elucidate the borylation mechanism. As shown in Fig. 2c, the observed ^{1}H NMR signals at 6.12, 5.20, and 4.43 ppm on the reaction mixture of

https://doi.org/10.1038/s41467-025-60674-9

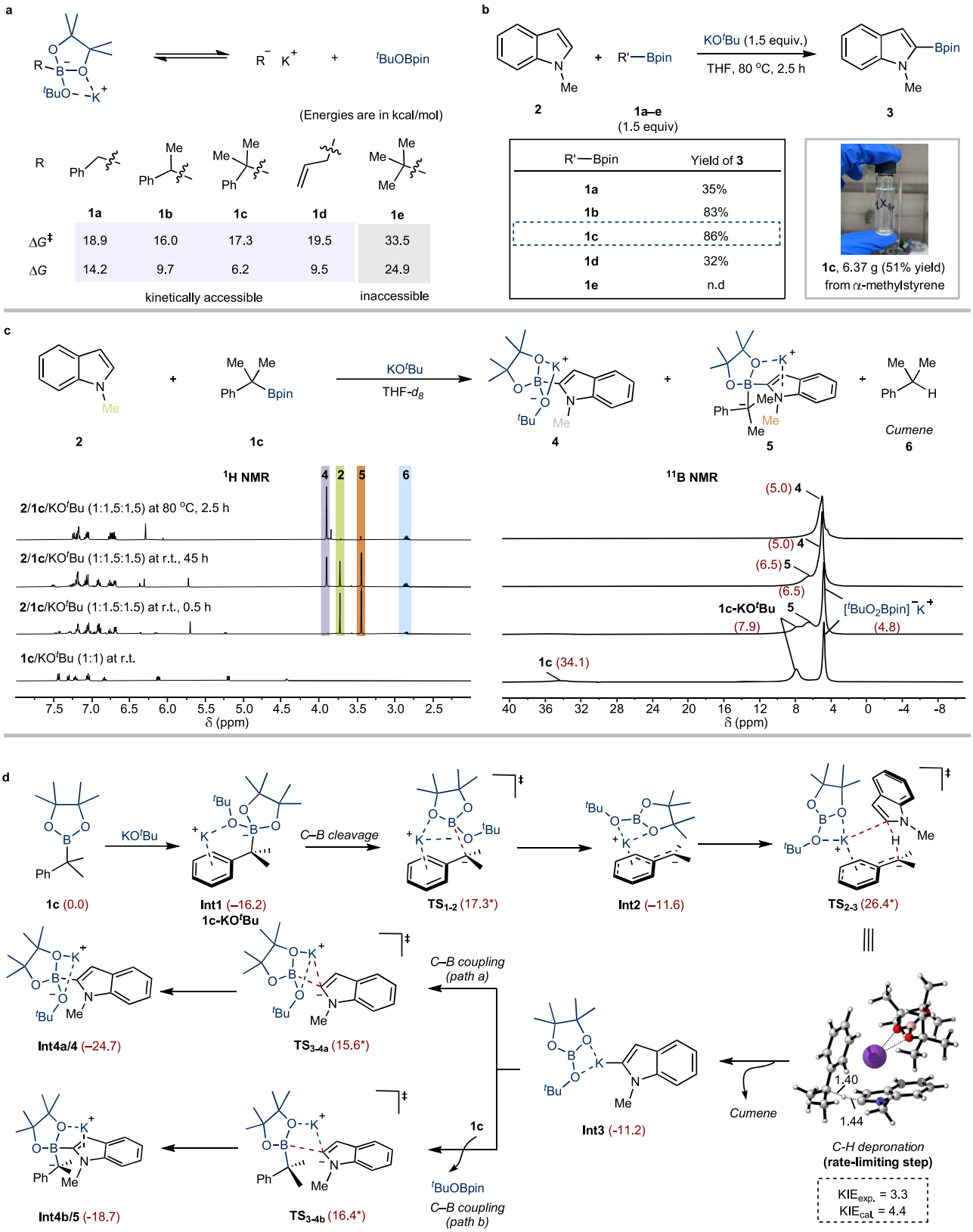

Fig. 2 | Exploration of the superbase reactivity of organboronates, application for aromatic C–H borylation reaction, and mechanistic insight. **a** Computational screening for the possible organoboronates/KO^{t}Bu combination, which could undergo C–B bond heterolysis to generate carbanion species ($\Delta G^{\ddagger}$: activation barrier; ΔG: reaction energy). **b** Experimental evaluation of the reactivity of different organoboronates for the C–H borylation of N-methylindole **2**. **c** ^{1}H and ^{11}B NMR (400 MHz, THF-d_8) studies on the model reaction. Numbers within the parentheses are the boron resonances. **d** Computed pathways [M06-2X/def2-TZVPP, SMD(THF)//M06-2X/def2-SVP, SMD(THF)] for C–H borylation of N-methylindole with benzylic boronate **1c**/KO^{t}Bu combination. The Gibbs free reaction energies (relative to **1c**) and barriers (labeled with an asterisk, relative to **Int1**) are in kcal mol^{-1}. KIE: Kinetic Isotope Effect ($KIE_{exp.}$: experimental measured KIE; $KIE_{cal.}$: computed KIE with **TS$_{2\text{-}3}$**). Color code: H, white; C, gray; B, pink; O, red; N, blue; K, purple.

1c/KO^{t}Bu confirms the formation of the benzylic carbanion species[16] (see Supplementary Fig. 8). The detection of cumene as a by-product in the borylation reaction mixture identified the deprotonation metalation process, which could also be supported by the borylation reaction using independently synthesized dimethyl benzylic potassium ($PhCMe_2K$) as the base (Supplementary Fig. 5). Replacing dimethyl benzylboronate **1c** with ^{i}PrOBpin, which is a commonly used boron source for the deprotonative borylation of arenes with organometallic reagents[25], failed to yield any borylation product (Supplementary Fig. 6). This outcome might be attributed to the irreversible binding of ^{i}PrOBpin to KO^{t}Bu. For the reaction mixture at room temperature, two distinct types of ate complexes **4** and **5** (formed by complexation of borylation product **3** with KO^{t}Bu and dimethyl benzylic carbanion, respectively) could be detected on the ^{1}H NMR and ^{11}B NMR spectrum (Supplementary Figs. 10–11 for detailed characterization). ^{11}B NMR analysis on the mixture of $PhCMe_2K$ with borylation product **3** provides spectroscopic evidence for the formation of carbanion-indole borate complex **5** in the reaction mixture (Supplementary Fig. 12). Despite extending the reaction time to 45 h at room temperature, the indole reactant did not achieve complete conversion. When the reaction mixture was heated to 80 °C, the KO^{t}Bu-bounded indole borate **4** became the predominant species, with only a small amount of species **5**. This suggests that the formation of the tetracoordinated borylation product **4** is thermodynamically more favorable than that of the other ate complex **5**. Furthermore, the detection of cumene **6** as a by-product in the borylation reaction mixture implied the involvement of a deprotonation metalation process.

Density functional theory (DFT) calculations were performed on the model reaction involving benzylic boronate **1c**, N-methylindole **2**, and KO^{t}Bu, indicating that the deprotonative borylation mechanism is both kinetically and thermodynamically feasible (Fig. 2d and Supplementary Fig. 36). Competing pathways, such as C2–H and C3–H deprotonative borylation as well as carbanion addition/ring-opening pathway, were systematically identified using our combined molecular dynamics and coordinate driving methods[26,27] (Supplementary Figs. 40–41). Among these, the C2–H deprotonative borylation pathway is identified as the most kinetically favorable path. This deprotonative metalation/borylation mechanism resembles the ionic mechanisms involved in the KO^{t}Bu-catalyzed C–H bond silylation of aromatic heterocycles[28,29]. The borylation reaction starts with the complexation of KO^{t}Bu with **1c**, resulting in the formation of the ate complex **Int1**. **Int1** then undergoes C–B bond heterolysis through transition state $\mathbf{TS_{1\text{-}2}}$ to yield the zwitterionic complex **Int2**. This complex comprises a benzylic potassium fragment and a boronate ester fragment (^{t}BuOBpin). The kinetic feasibility of this process is supported by NMR analysis (Supplementary Fig. 8). Subsequently, the benzylic potassium fragment of **Int2** deprotonates the C2–H of indole, leading to the formation of the C–H metalation intermediate **Int3** (^{t}BuOBpin-K-indole) with an activation barrier of 26.4 kcal mol^{-1} (via $\mathbf{TS_{2\text{-}3}}$, relative to **Int1**). Potassium indole **Int3** can react with either ^{t}BuOBpin or **1c**, affording ate complexes **Int4a** (**4**) and **Int4b** (**5**), respectively. Both of these pathways are kinetically accessible, with activation barriers of 15.6 and 16.4 kcal mol^{-1} for the transition states $\mathbf{TS_{3\text{-}4a}}$ and $\mathbf{TS_{3\text{-}4b}}$, respectively. The ^{t}BuO-indole borate complex (**Int4a**) is predicted to be more thermodynamically favorable by 6.0 kcal mol^{-1} compared to the dimethyl benzylic carbanion-indole borate complex (**Int4b**), aligning with our experimental observations (c.f., Fig. 2c). Given that the initial concentration of **1c** is significantly higher than that of ^{t}BuOBpin, it is likely that the predominant C–B coupling process at room temperature might involve the reaction of potassium indole (K-indole) with **1c**. Along the whole borylation process, the C2–H deprotonation step is the rate-limiting step with an overall free-energy barrier of 26.4 kcal mol^{-1}. Parallel kinetic isotope effect (KIE) experiments also reveal a pronounced KIE value of 3.3 ($KIE_{cal.} = 4.4$), providing further support for the DFT calculations. Additionally, our calculations show that the cation-π interaction between the K^+ cation and the indole ring can significantly lower the energy barrier of C–H deprotonation transition state (Supplementary Fig. 38). The addition of 18-crown-6 to complex with the K^+ cation reduced the borylation yields (Supplementary Fig. 7), suggesting the crucial role of cation-π interactions in the related transition states. Further computational comparative analysis on the reaction with LiO^{t}Bu and NaO^{t}Bu through DFT calculations elucidates the critical role of K^+ in mediating indole deprotonation processes (Supplementary Fig. 42). Besides, the solvent coordination effect was also computationally investigated. It was found that THF-solvated microscopic states are also likely to co-exist in the reaction system (Supplementary Fig. 43). In addition, we also computationally investigated C–H borylation reaction of N-methylindole with **1d** as the boron source. It was found that the reaction of **1d** with N-methylindole requires a noticeably higher activation barrier in the C–H deprotonative step (see Supplementary Fig. 44 for the computed free energy profile).

Synthetic scope for regioselective C–H borylation reaction

The selection of boron source for the deprotonation borylation of different aromatic compounds can be customized according to the C–H bond acidity in the substrates. An experimental study involving a 3 × 4 matrix, which comprises 3 (hetero)aromatic substrates (N-methylindole, methoxybenzene, 2,3-benzofuran) and 4 boronate reagents (**1a**-**1d**), has established a general guideline for choosing appropriate substrate-boronate combinations (Supplementary Fig. 22). N-methylindole, with a moderate C2–H pK_a value of 37.2, can be efficiently borylated by both methyl and dimethyl benzylic boronate (**1b** and **1c**) to yield products with excellent yields. In contrast, methoxybenzene with a higher *ortho*-C–H pK_a value of 41.3, only reacts with dimethyl benzylic boronate **1c** to afford the borylation product. For the more reactive 2,3-benzofuran, with a C2–H pK_a of 32.7, both benzylic boronate **1a** and allylic boronate **1d** are suitable boron sources for the borylation reaction. DFT calculations can differentiate the reactivity of these different combinations and have shown that the activation barriers are well-correlated with the calculated pK_a values (Supplementary Fig. 45).

Following a substrate-adaptive investigation, the substrate scope for the borylation reaction was explored. Generally, the borylation reaction occurs at the most acidic position of the substrate. As illustrated in Fig. 3a, substrates with pK_a values between 34.5 and 41.3 can be effectively borylated using benzylic boronate **1c**. A range of N-substituted indoles, including those with methyl (Me), ethyl (Et), and phenyl (Ph) groups, all undergo regioselective C2–H borylation with moderate to good yields (**3, 7**-**8**). The scalability of this method is exemplified by a 5 mmol scale synthesis using N-methylindole, demonstrating the practicality of this method. Despite the benzylic C(sp^3)–H bonds being more acidic than C(sp^2)–H bonds, the borylation of methylated indoles proceeds with complete chemoselectivity at the sp^2 hybridized C–H positions (**10**,**12**-**13**). DFT calculations reveal that the observed chemoselectivity is thermodynamically dictated, with C(sp^2)–B bond formation being energetically favored over the formation of benzylic boronate (see Supplementary Fig. 46 for computational details). Furthermore, a variety of substituents at different positions on the indole framework, such as methyl, methoxy, fluoro, chloro, and trifluoromethyl, are well-tolerated, affording the desired products **9**-**17** in yields ranging from 43% to 76%. Although the C(sp^2)–H borylation of aromatic compounds has been well established (for example, using iridium catalysts)[30–33], the regioselective borylation reaction is typically achieved by employing a directing group strategy[34–37] or ligand engineering[38–41]. In contrast, our method selectively targets the most acidic C(sp^2)–H bonds of the substrates, leading to excellent regioselectivity in borylation. In addition, this approach offers a distinct, orthogonal strategy compared to borylation processes through the electrophilic borylation mechanism[42–44].

https://doi.org/10.1038/s41467-025-60674-9

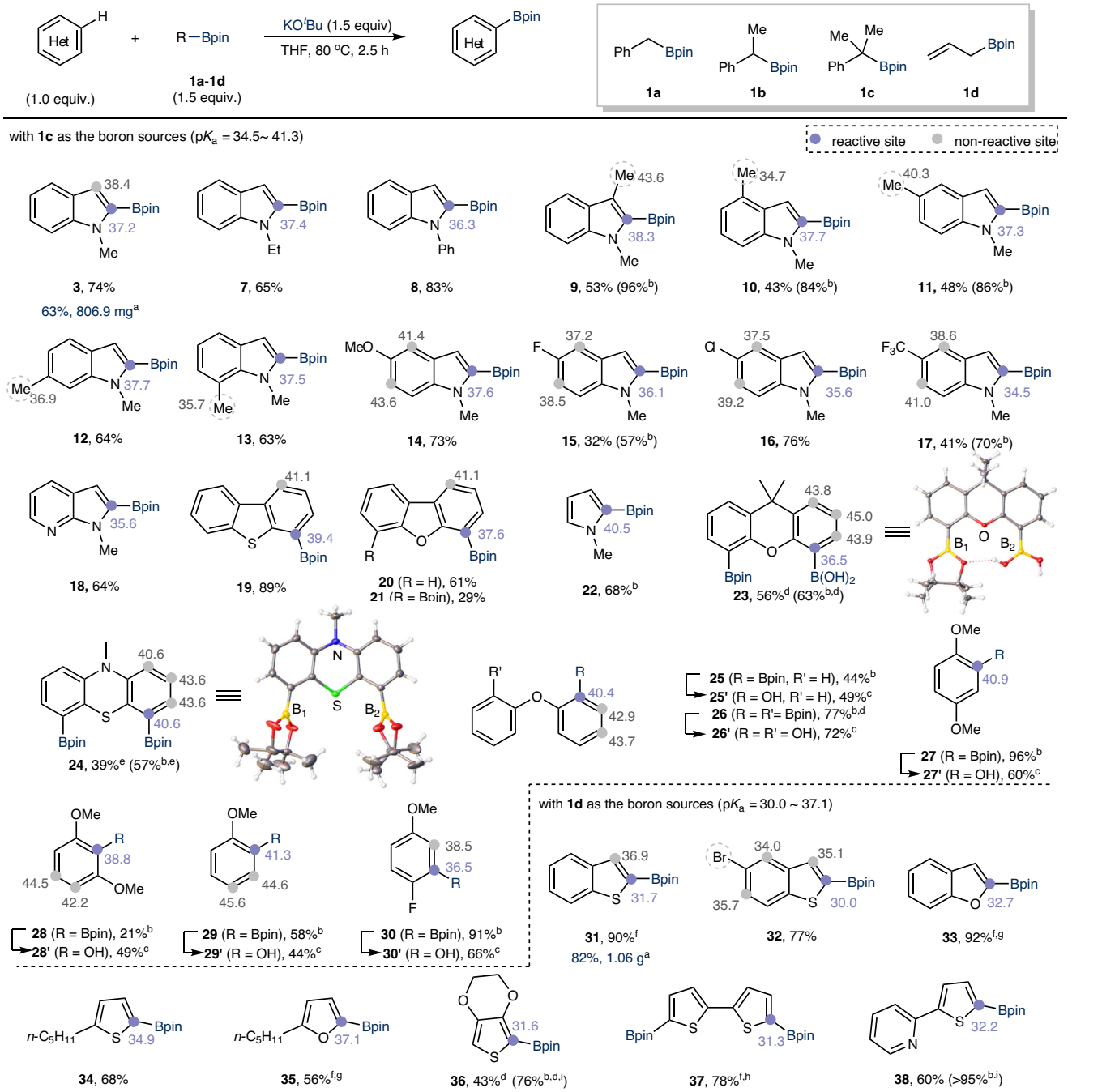

Fig. 3 | Substrate scope for the C–H borylation of (hetero)arenes. The numbers labeled on the arenes are the calculated pK_a values of the related C–H bonds. Reaction conditions: substrates (0.2 mmol), **1c** or **1d** (1.5 equiv.), KO^{t}Bu (1.5 equiv.) in 1.0 mL of THF at 80 °C, 2.5 h, under Ar. [a]5 mmol scale. [b]Yield determined by ^{1}H NMR due to the product decomposition during the purification. [c]Cascade C–H borylation/hydroxylation: $NaBO_3{\cdot}4H_2O$ (3.0 equiv.), THF/H_2O = 1:1 at room temperature, 3 h. [d]**1c** or **1d** (3.0 equiv.) and KO^{t}Bu (3.0 equiv.). [e]**1c** (4.2 equiv.) and KO^{t}Bu (4.2 equiv.). [f]Without further purification by column chromatography on silica gel. [g]**1d** (1.1 equiv.) was used. [h]**1d** (2.2 equiv.) and KO^{t}Bu (2.5 equiv.). [i]At 60 °C, 2.5 h. Color code: H, white; C, gray; B, yellow; O, red; N, blue; S, green.

Furthermore, this strategy for C–H borylation can be extended to other heteroarenes commonly found in bioactive molecules, including 7-azaindole, dibenzothiophene, dibenzofuran, and pyrrole, affording the related mono- or bis-borylated products in good to excellent yields (**18**–**22**). The diborylation of 9,9-dimethylxanthene derivative **S23** and phenothiazine derivative **S24** proceeded effectively using 3 - 4 equivalents amount of boron source, affording the corresponding diborylation products **23** and **24** in moderate yields (63% and 57% NMR yields, respectively). Notably, X-ray crystallographic analysis of the 9,9-dimethylxanthene derived product **23** revealed two divergent boron substitution patterns, providing structural flexibility that enables regioselective elaboration in downstream synthesis. C–H borylation of aryl ethers could also be achieved, yielding the corresponding *ortho*-borylation products in moderate to good yields (**25**–**30**). 1,3-dimethoxybenzene (**S28**), which poses significant steric hindrance and is challenging through traditional transition-metal-catalysis[45], could also be borylated to produce **28**. It has been shown that aryl fluorides readily undergo nucleophilic substitution reaction when treated with benzylic organoboronates and alkoxide base, affording C–C coupling product[46]. However, for 4-fluoroanisole (**S30**), the C–H borylation

reaction is favorable, and preferentially occurred at the *ortho*-position relative to the fluorine group. The observed regioselectivity might be attributed to the increased acidity of the C−H bond *ortho* to the fluorine atom[47,48], rather than by complex-induced proximity effects (CIPE)[49]. Given the high susceptibility of aryl ether boron compounds to decomposition during separation processes[50], we adopted a two-stage borylation/oxidative hydroxylation protocol to directly transform the borylation product into phenol derivatives (**25′-30′**), which are frequently found in natural products and pharmaceuticals[51].

For O- and S-containing heteroaromatics with lower pK_a (30.0 - 37.1), the commercially available allyl pinacol boronate **1d** could also serve as an optimal boron source for the borylation reactions (**31**–**38**). This includes the synthesis of building blocks for organic photo-electric materials[52], such as borylated benzothiophenes and thiophenes (**31, 37**). Since propylene is the sole by-product (Supplementary Fig. 13), the borylation product can be conveniently obtained through a series of quenching → extraction → solvent recycling steps (e.g., **31, 33, 35**, and **37**). In addition, the borylation of benzothiophene can be scaled up to a 5 mmol reaction, yielding the desired product in 86% yield. While the aryl C−Br bond is typically reactive in the presence of organolithium reagents, it remains intact when using the combination of **1d**/KO^{t}Bu for the borylation of 5-bromobenzo[*b*]thiophene (**32**). Notably, treatment of 1-methylindazole with boronate/KO^{t}Bu combinations (**1c** or **1d**) under standard conditions did not produce the anticipated borylation product. Instead, the pyrazole ring undergoes a ring-opening reaction to afford a benzonitrile derivative (Supplementary Fig. 15). This reaction outcome is consistent with previous studies of 1-methylindazole decomposition reaction in the presence of organolithium/magnesiums[53]. These reaction outcomes provide another evidence for the organometallic-like reactivity inherent to boronate/KO^{t}Bu combinations. In addition, we also explored other heterocyclic substrates (e.g., benzothiazoles, benzoxazoles, and benzimidazoles etc.) with low pK_a values. However, the reactions of these heterocycles failed to form the corresponding boronate esters. These outcomes may stem from the existence of other unidentified competing pathways specific for these substrates (see Supplementary Fig. 54 for a collection of unsuccessful substrates).

Machine learning (ML) methodologies have recently been proven to be highly valuable in synthetic chemistry, including reaction outcome prediction, retrosynthetic route planning and catalyst design[54–59]. We, therefore, employed ML to explore the substrate adaptivity across diverse (hetero)arene/boronate combinations. To ensure the generalizability of the model, iterative training strategy was adopted (see Supplementary Fig. 56). After two rounds of model iteration, the generalizability of the model was significantly improved as evidenced by the decreasing of mean absolute error (MAE) on the external validation set from 29.0% to 15.4% (Fig. 4a). Algorithm screening through comparative analysis demonstrated that Support Vector Regression (SVR) exhibited significant predictive superiority relative to alternative machine learning architectures within our experimental dataset (Fig. 4b and Supplementary Tables 9–11 for details). Feature importance analysis revealed that the LUMO energy of the boronate compound and the charge of the hydrogen atom on the (hetero)arene (which might be related to the C−H deprotonative process) are the most critical descriptors for reactivity prediction (Fig. 4c). The final model results (Fig. 4d) demonstrate that while our targeted data augmentation successfully captured greater chemical heterogeneity, this approach led to a slightly increase of MAE in the training set (from 7.6% to 12.5%). The observed decline in model accuracy likely stems from the introduction of chemically distinct motifs absent in the initial training set (such as benzoxazole, a substrate with a relatively low pK_a of 25.1). Introducing such chemically diverse samples could exacerbate data heterogeneity, given that the original dataset is predominantly clustered around pK_a values of about 30 - 47. Figure 4e exemplified the predictive ability of our optimized model through experimental verification. For instance, it accurately predicted a favorable outcome for the unseen substrate N-methylpyrazole using **1d** as the boron source (**S40**, 39% predicted yield and 43% observed yield). Besides, it exhibited satisfactory accuracy in boron source selection: for 5-fluoro-1-methyl-1*H*-indole, the model correctly prioritized **1b** over **1c** (63% versus 57%), while for 1-methyl-7-azaindole, the **1b**-mediated system showed superior experimental yields (78% versus 64% with **1c**). Both cases are in good consistence with computational predictions. However, the model underestimated the yield for 4-fluoro-N,N-dimethylaniline (**S39**), predicting 29% yield versus an experimental yield of 75% (with **1c**). This discrepancy might stem from the limited number of examples with similar substitution patterns in the training data, hindering the model's ability to effectively capture the competing electronic influences exerted by the amino and fluoro substituents on the substrate. Overall, through iterative data augmentation strategies, we progressively enhanced the model's generalization capabilities, enabling more robust predictions across extensive and diverse chemical space.

Synthetic application and scope extension

We then investigated the application of this strategy for the functionalization of high-value-added arenes. Axially chiral 1,1′-bi-2-naphthol (BINOL) derivative **S42**[60], a crucial ligand in asymmetric catalysis, readily reacted with **1c** to yield the 3,3′-bisborylated product **42** in 76% yield on a 1.0 mmol scale (Fig. 5a). While this transformation was previously achievable using ^{n}BuLi through a two-stage deprotonation/borylation process[61], it necessitated cryogenic conditions and careful handling of the sensitive ^{n}BuLi reagent. The antiplatelet agent ticlopidine **S43** underwent C−H borylation to yield the borylated product **43** in excellent yield (Fig. 5b). Given that this borylation approach yields tetracoordinated aryl boronates, it can be directly utilized in palladium-catalyzed Suzuki-Miyaura cross-coupling reactions[14], offering a step-economical route for drug modification (**44**–**46**). For instance, employing 1,2-bis(4-bromophenyl)diazene (λ_{max} = 335 nm) as the coupling reagent, a bis-coupling product was obtained in high yield. The unique light absorption characteristics of **46** (λ_{max} = 413 nm, Supplementary Fig. 24), suggest its potential application in the field of photopharmacology[62]. Moreover, (−)-menthol derivative **S47** and (±)-α-tocopherol derivative **S48** proceeded well under standard conditions using **1d** as the boron source, affording the borylated products **47** and **48** in 63% and 83% yields, respectively.

To further showcase the versatility of our method, we extended its application to dehalogenative borylation reactions, which are commonly conducted with organometallic reagents or via Miyaura borylation[63,64]. A two-stage borylation followed by Suzuki-Miyaura coupling demonstrated the applicability of this strategy in the borylation of aryl bromides (Fig. 5c). We also performed DFT calculations on the mechanism of debromoborylation (see Supplementary Fig. 48 for computational details). While 1,1-bis[(pinacolato)boryl]alkanes have been reported for the borylation of aryl and vinyl halides, their reactions with aryl bromides typically exhibit low efficiency[65]. Utilizing 1-phenylethyl boronate (**1b**) as the boron source, a wide range of aryl bromides could be successfully borylated and subsequently coupled with 2-bromopyridine via palladium catalysis, yielding the corresponding biaryls in moderate to excellent yields (**49**–**65**). A range of functional groups, including dimethyl amine (**55**), benzyl-protected phenol (**57**), *tert*-butyldimethylsilyl (TBS) protected alcohol (**58**), amide (**62**) and heterocycles (**63**–**65**), were found to be compatible with this process. In addition, aryl iodide 4-iodoanisole could also undergo a cascade borylation/Suzuki-Miyaura process to produce the biaryl product (**56**) with good yield. DFT calculations on different *para*-halogenated anisoles (Supplementary Fig. 51) revealed differences in reactivity and selectivity among the various *para*-halogenated anisoles. Performing the stereochemical scrambling experiments with the

https://doi.org/10.1038/s41467-025-60674-9

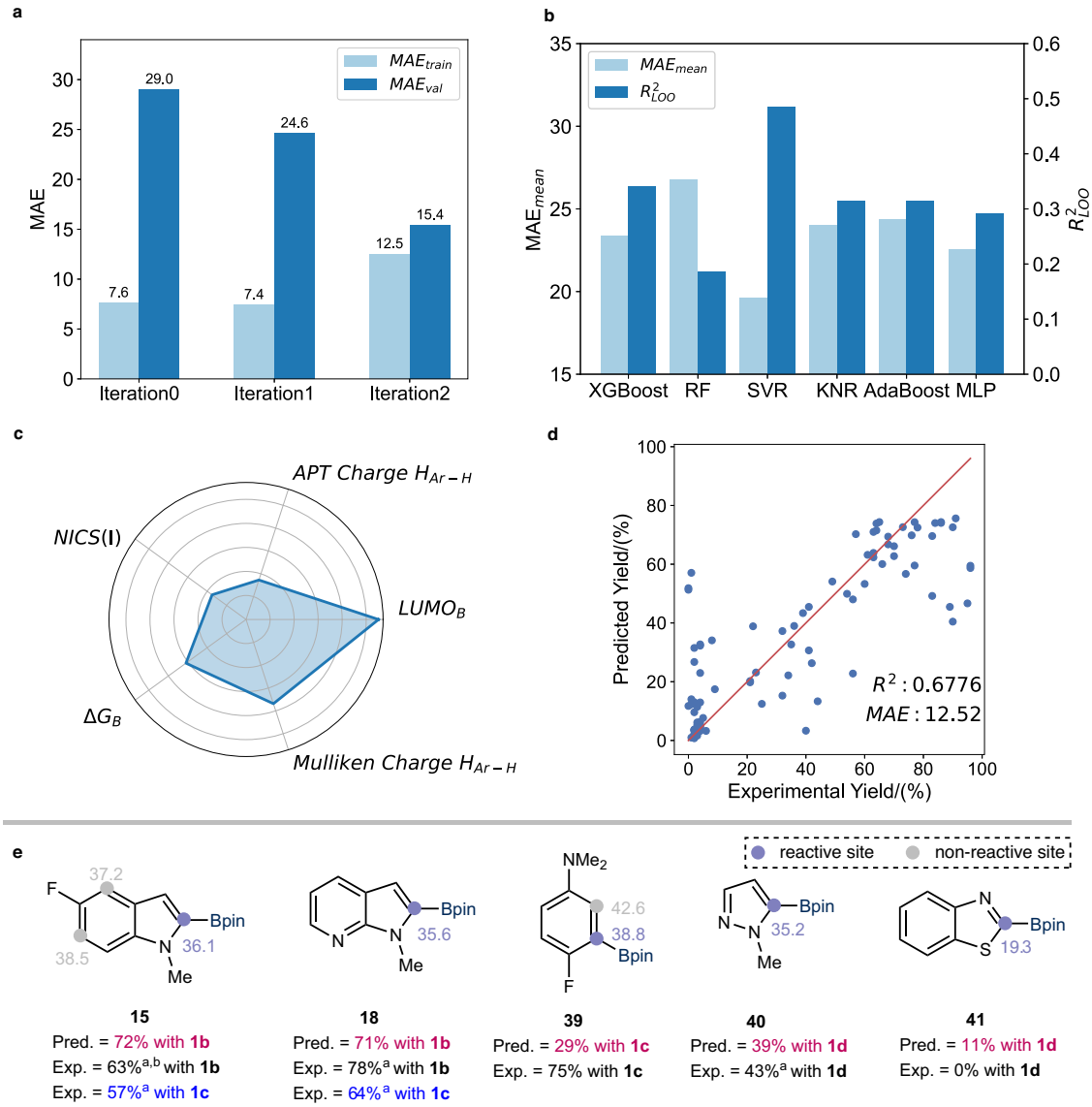

Fig. 4 | Development, analysis, and predictive application of a machine learning model for borylation reactivity. a Model performance (training and validation) across iterative data augmentation rounds. **b** Comparative performance of different ML algorithms leading to the selection of SVR. **c** Feature importance analysis identifying critical descriptors for the final SVR model. **d** Performance of the final SVR model for reactivity prediction. **e** Machine learning predictions for external examples and experimental verification. Reaction conditions: substrates (0.2 mmol), **1c, 1b** or **1d** (1.5 equiv.), KO^{t}Bu (1.5 equiv.) in 1.0 mL of THF at 80 °C, 2.5 h, under Ar. [a]Yield determined by ^{1}H NMR. The numbers labeled on the arenes are the calculated pK_a values of the related C–H bonds. (Pred.: Predicted yield; Exp.: Experimental yield).

enantioenriched chiral substrate (***R***)-**1b** leads to the formation of **1b'** with complete loss of chirality (see Supplementary Fig. 19 for details). These experiments confirm that the elementary debromination step inherently involves a free carbanion-mediated pathway.

In a final effort to establish the generality of in situ superbase generation strategy, we turned our attention to the anionic polymerization of styrene, another significant application of organometallic reagents (Fig. 5d and see Supplementary Fig. 23 for the characterization of polymers). Employing a 20 mol% mixture of **1c**/KO^{t}Bu as the initiator, 4-chlorostyrene was polymerized to yield polystyrene **66** (Mn: 22.9 kDa; polydispersity index, PDI: 2.51) in 63% yield. More importantly, the molecular weight of the resulting polymerization can be readily controlled by varying the amount of initiator. Reducing the amount of initiator to 10 mol% and 5 mol% led to a significant increase in the number-average molecular weight (Mn) of polystyrenes, from 22.9 kDa to 98.1 and 166.7 kDa, respectively. This in situ generated superbase approach is expected to provide a new strategy for the controlled polymerization of styrene.

Discussion

The results presented here demonstrate that the superbase reactivity of classical organometallic reagents can be readily achieved through the use of stable benzylic or allylic boronates in combination with alkali-metal alkoxides. This provides a unique tool for the construction of C(sp^2)–B bonds, proceeding through either regioselective C–H deprotonation or metal-halogen exchange mechanistic scenarios. The diverse structures of boronates facilitate the fine selection of substrate combinations. This method is also applicable to the controlled polymerization of styrene. This in situ-generated carbanions strategy overcomes the synthetic and storage issues associated with traditional organometallic reagents. We believe the diverse reactivity of this method will likely be of great utility to the fields of organic synthesis

https://doi.org/10.1038/s41467-025-60674-9

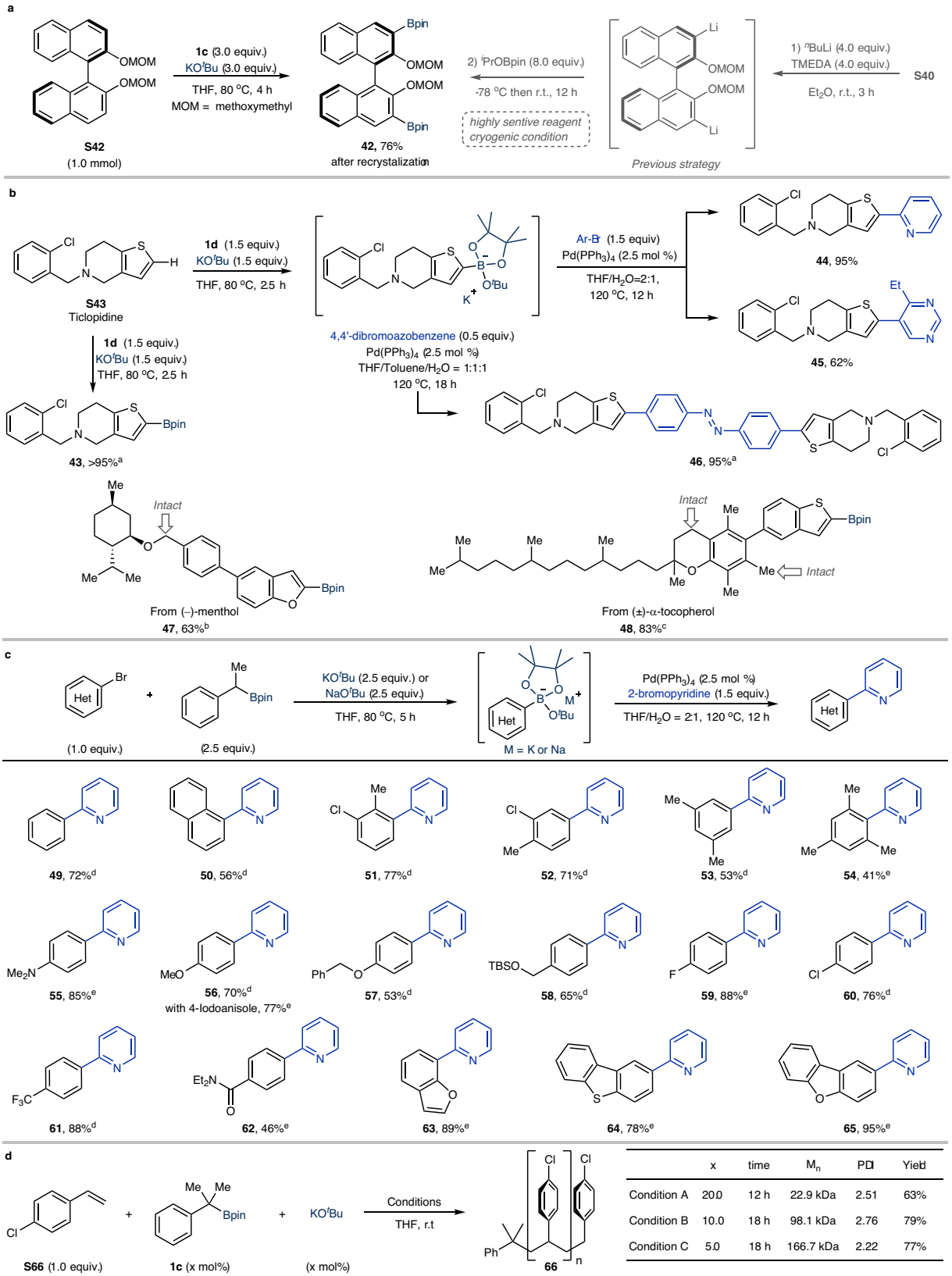

	x	time	M_n	PDI	Yield
Condition A	20.0	12 h	22.9 kDa	2.51	63%
Condition B	10.0	18 h	98.1 kDa	2.76	79%
Condition C	5.0	18 h	166.7 kDa	2.22	77%

Fig. 5 | Application of the (hetero)arenes C(sp^2)–H borylation and scope extension to borylation of aryl bromides and anionic polymerization. **a** Borylation of methoxylmethyl (MOM)-protected (*R*)-BINOL and a comparison to the previous strategy. **b** Cascade C(sp^2)–H borylation/Suzuki-Miyaura cross-coupling for the structural diversification of drug-relevant substrates. **c** Cascade borylation of aryl bromides/Suzuki-Miyaura cross-coupling for the synthesis of biaryls. **d** Benzylic boronate/KO^{t}Bu combination-initiated polymerization of 4-chlorostyrene under different conditions. [a]Without further purification by column chromatography on silica gel. [b]**S47** (0.2 mmol), **1d** (1.1 equiv) and KO^{t}Bu (1.5 equiv) in 1.0 mL of THF at 40 °C, 5 h, under Ar. [c]**S48** (0.1 mmol), **1d** (1.5 equiv) and KO^{t}Bu (1.5 equiv) in 1.0 mL of THF at 60 °C, 5 h, under Ar. [d]With KO^{t}Bu. [e]With NaO^{t}Bu.

and medicinal chemistry, and that the practicality of the borylation reaction will lead to broader synthetic applications, especially through the use of tandem processes.

Methods

General procedure for C–H borylation reaction of (hetero)arenes for the synthesis of arylboronates

In an argon-filled glovebox, bases (0.15 mmol ~ 0.3 mmol, 1.5 equiv. ~ 3.0 equiv.), boron sources **1c** or **1d** (0.15 mmol ~ 0.3 mmol, 1.5 equiv. ~ 3.0 equiv.) and THF (0.5 ~ 1.0 mL) were added to an oven-dried 10 mL Schlenk tube equipped with a magnetic stir bar. The resulting mixture was pre-stirred at ambient temperature for 10 min, and then the corresponding (hetero)arenes (0.1 mmol ~ 0.2 mmol, 1.0 equiv.) were added into the reaction mixture. The reaction tube was sealed, removed from the glovebox and stirred at the indicated temperature for 2.5 ~ 5 h. After the reaction finished, saturated NH_4Cl solution (3 mL) and saturated brine (1.0 mL) were added to the reaction mixture, and the organic phase was separated. The aqueous phase was extracted with diethyl ether (3 × 3 mL). Then, the organic phases were combined, dried over anhydrous Na_2SO_4, and filtered. After the removal of the solvent under reduced pressure, the crude material was purified by flash column chromatography on silica gel or preparative thin-layer chromatography to afford the corresponding borylation products.

General procedure for cascade C–H borylation/hydroxylation of aryl ether for the synthesis of phenol derivatives

Step 1. C–H borylation. In an argon-filled glovebox, KO^{t}Bu (3.0 mmol ~ 6.0 mmol, 1.5 equiv. ~ 3.0 equiv.), **1c** (3.0 mmol ~ 6.0 mmol, 1.5 equiv. ~ 3.0 equiv.) and THF (0.5 ~ 1.0 mL) were added to an oven-dried 10 mL Schlenk tube equipped with a magnetic stir bar. The resulting mixture was pre-stirred at ambient temperature for 10 min, and then the corresponding aryl ethers (0.2 mmol, 1.0 equiv.) were added to the reaction mixture. The reaction tube was sealed, removed from the glovebox and stirred at 80 °C for 2.5 h.

Step 2. Then, C–B hydroxylation. After the reaction finished, the reaction mixture was cooled to room temperature, and $NaBO_3{\cdot}4H_2O$ (0.6 mmol ~ 1.2 mmol, 3.0 ~ 6.0 equiv.) and H_2O (1.0 mL) were added into the reaction mixture. The mixture was stirred for an additional 3 h at room temperature. Then, saturated NH_4Cl solution (3 mL) and saturated brine (1.0 mL) were added to the reaction mixture, and the organic phase was separated. The aqueous layer was extracted with ethyl acetate (3 × 3 mL). Then, the organic layers were combined, dried over anhydrous Na_2SO_4, and filtered. After the removal of the solvent under reduced pressure, the crude material was purified by preparative thin-layer chromatography to afford the corresponding phenol derivatives.

General procedures for cascade borylation of aryl bromides/Suzuki-Miyaura cross-coupling for the synthesis of biaryl products

Step 1. Debromoborylation. In an argon-filled glovebox, KO^{t}Bu (56.0 mg, 0.5 mmol, 2.5 equiv.) or NaO^{t}Bu (48.0 mg, 0.5 mmol, 2.5 equiv.), methyl benzylic boronate **1b** (116.0 mg, 0.5 mmol, 2.5 equiv.) and THF (1.0 mL) were added to an oven-dried 10 mL Schlenk tube equipped with a magnetic stir bar. The resulting mixture was pre-stirred at ambient temperature for 10 min, then aryl bromides (0.2 mmol, 1.0 equiv.) were directly added to the reaction mixture. The reaction tube was sealed and stirred at 80 °C for 5 h.

Step 2. Suzuki-Miyaura cross-coupling. After the borylation process finished, $Pd(PPh_3)_4$ (5.8 mg, 0.05 mmol, 0.025 equiv.), 2-bromopyridine (47.4 mg, 0.3 mmol, 1.5 equiv.) and degassed water (0.5 mL) were added to the reaction mixture. The reaction tube was sealed, removed from the glovebox and stirred at 120 °C for 12 h. After the reaction finished, saturated NH_4Cl solution (3 mL) and saturated brine (1.0 mL) were added to the reaction mixture, and the organic phase was separated. The aqueous layer was extracted with ethyl acetate (3 × 3 mL). Then, the organic layers were combined, dried over anhydrous Na_2SO_4, and filtered. After the removal of the solvent under reduced pressure, the crude material was purified by preparative thin-layer chromatography to afford the corresponding biaryl products.

Data availability

The authors declare that all other data supporting the findings of this study are available within the article and Supplementary Information files, and are also available from the corresponding authors upon request. The X-ray crystallographic structure data generated in this study have been deposited in the Cambridge Crystallographic Data Center (CCDC) database under accession code 2443058 (**23**) and 2443061 (**24**), and can be obtained free of charge via https://www.ccdc.cam.ac.uk/structures/. The final dataset for yield prediction model labeled as Data-round-ML and the cartesian coordinates of DFT-calculated geometries labeled as xyz-coordinates in this study are provided in the Source Data file. Source data are provided with this paper.

Code availability

The source codes generated during the current study are available at https://github.com/Daojing-Li/Stable-Organoboronates-ML-Supp.

References

1. Schlosser, M. *Organometallics in Synthesis: Third Manual*. (John Wiley & Sons, Inc., 2013).
2. Reich, H. J. Role of organolithium aggregates and mixed aggregates in organolithium mechanisms. *Chem. Rev.* **113**, 7130–7178 (2013).
3. Robertson, S. D., Uzelac, M. & Mulvey, R. E. Alkali-metal-mediated synergistic effects in polar main group organometallic chemistry. *Chem. Rev.* **119**, 8332–8405 (2019).
4. Tilly, D., Chevallier, F., Mongin, F. & Gros, P. C. Bimetallic combinations for dehalogenative metalation involving organic compounds. *Chem. Rev.* **114**, 1207–1257 (2014).
5. Vidal, C., García-Álvarez, J., Hernán-Gómez, A., Kennedy, A. R. & Hevia, E. Exploiting deep eutectic solvents and organolithium reagent partnerships: Chemoselective ultrafast addition to Imines and quinolines under aerobic ambient temperature conditions. *Angew. Chem. Int. Ed.* **55**, 16145–16148 (2016).
6. Slavík, P., Trowse, B. R., O'Brien, P. & Smith, D. K. Organogel delivery vehicles for the stabilization of organolithium reagents. *Nat. Chem.* **15**, 319–325 (2023).
7. Mulks, F. F. et al. Continuous, stable, and safe organometallic reactions in flow at room temperature assisted by deep eutectic solvents. *Chem* **8**, 3382–3394 (2022).
8. Weidmann, N., Harenberg, J. H. & Knochel, P. Continuous flow preparation of (Hetero)benzylic Lithiums via iodine–Lithium exchange reaction under Barbier conditions. *Org. Lett.* **22**, 5895–5899 (2020).
9. Yang, K. & Song, Q. Tetracoordinate boron intermediates enable unconventional transformations. *Acc. Chem. Res.* **54**, 2298–2312 (2021).
10. Fyfe, J. W. B. & Watson, A. J. B. Recent developments in organoboron chemistry: Old dogs, new tricks. *Chem* **3**, 31–55 (2017).
11. Xu, L., Zhang, S. & Li, P. Boron-selective reactions as powerful tools for modular synthesis of diverse complex molecules. *Chem. Soc. Rev.* **44**, 8848–8858 (2015).
12. Miyaura, N. & Suzuki, A. Palladium-catalyzed cross-coupling reactions of organoboron compounds. *Chem. Rev.* **95**, 2457–2483 (1995).

13. Lennox, A. J. J. & Lloyd-Jones, G. C. Selection of boron reagents for Suzuki–Miyaura coupling. *Chem. Soc. Rev.* **43**, 412–443 (2014).
14. Suzuki, A. Cross-coupling reactions of organoboranes: An easy way to construct C–C bonds (Nobel Lecture). *Angew. Chem. Int. Ed.* **50**, 6722–6737 (2011).
15. Boudier, A., Bromm, L. O., Lotz, M. & Knochel, P. New applications of polyfunctional organometallic compounds in organic synthesis. *Angew. Chem. Int. Ed.* **39**, 4414–4435 (2000).
16. Gao, L. et al. Base-mediated C–B bond activation of benzylic boronate for the rapid construction of β-silyl/boryl functionalized 1,1-diarylalkanes from aromatic alkenes. *Chem. Sci.* **14**, 11881–11889 (2023).
17. Hirao, A., Loykulnant, S. & Ishizone, T. Recent advance in living anionic polymerization of functionalized styrene derivatives. *Prog. Polym. Sci.* **27**, 1399–1471 (2002).
18. Goseki, R., Koizumi, T., Kurakake, R., Uchida, S. & Ishizone, T. Living anionic polymerization of 4-Halostyrenes. *Macromolecules* **54**, 1489–1498 (2021).
19. Kristensen, J., Lysén, M., Vedsø, P. & Begtrup, M. Synthesis of ortho substituted arylboronic esters by in situ trapping of unstable Lithio intermediates. *Org. Lett.* **3**, 1435–1437 (2001).
20. Leermann, T., Leroux, F. R. & Colobert, F. Highly efficient one-pot access to functionalized arylboronic acids via noncryogenic bromine/magnesium exchanges. *Org. Lett.* **13**, 4479–4481 (2011).
21. Bole, L. J., Tortajada, A. & Hevia, E. Enhancing metalating efficiency of the sodium amide NaTMP in arene borylation applications. *Angew. Chem. Int. Ed.* **61**, e202204262 (2022).
22. He, L. et al. Reaction condition- and functional group-specific knowledge discovery: Data- and computation-based analysis on transition-metal-free transformation of organoborons. *Artif. Intell. Chem.* **2**, 100034 (2024).
23. Liu, T. et al. Markovnikov-selective hydroboration of aryl alkenes enabled by a simple nickel salt. *Chin. J. Chem.* **40**, 2203–2211 (2022).
24. Research and Markets. *$542.9 Mn Alpha-Methylstyrene Market - Global Forecast to 2024* https://www.globenewswire.com/news-release/2019/05/27/1850397/0/en/542-9-Mn-Alpha-Methylstyrene-Market-Global-Forecast-to-2024.html (2019).
25. Hawkins, V. F., Wilkinson, M. C. & Whiting, M. Mild and selective synthesis of an aryl boronic ester by equilibration of mixtures of boronic and borinic acid derivatives. *Org. Process Res. Dev.* **12**, 1265–1268 (2008).
26. Yang, M., Zou, J., Wang, G. & Li, S. Automatic reaction pathway search via combined molecular dynamics and coordinate driving method. *J. Phys. Chem. A* **121**, 1351–1361 (2017).
27. Li, G. et al. Combined molecular dynamics and coordinate driving method for automatically searching complicated reaction pathways. *Phys. Chem. Chem. Phys.* **25**, 23696–23707 (2023).
28. Toutov, A. A. et al. Silylation of C–H bonds in aromatic heterocycles by an Earth-abundant metal catalyst. *Nature* **518**, 80–84 (2015).
29. Banerjee, S. et al. Ionic and neutral mechanisms for C–H bond silylation of aromatic heterocycles catalyzed by potassium tert-butoxide. *J. Am. Chem. Soc.* **139**, 6880–6887 (2017).
30. Wright, J. S., Scott, P. J. H. & Steel, P. G. Iridium-catalysed C–H borylation of heteroarenes: Balancing steric and electronic regiocontrol. *Angew. Chem. Int. Ed.* **60**, 2796–2821 (2021).
31. Nguyen, P., Blom, H. P., Westcott, S. A., Taylor, N. J. & Marder, T. B. Synthesis and structures of the first transition-metal tris(boryl) complexes: $(\eta^6$-Arene)Ir$(BO_2C_6H_4)_3$. *J. Am. Chem. Soc.* **115**, 9329–9330 (1993).
32. Ishiyama, T. et al. Mild Iridium-catalyzed borylation of arenes. high turnover numbers, room temperature reactions, and isolation of a potential intermediate. *J. Am. Chem. Soc.* **124**, 390–391 (2002).
33. Cho, J.-Y., Tse, M. K., Holmes, D., Maleczka, R. E. & Smith, M. R. Remarkably selective iridium catalysts for the elaboration of aromatic C-H bonds. *Science* **295**, 305–308 (2002).
34. Robbins, D. W., Boebel, T. A. & Hartwig, J. F. Iridium-catalyzed, silyl-directed borylation of nitrogen-containing heterocycles. *J. Am. Chem. Soc.* **132**, 4068–4069 (2010).
35. Snieckus, V. Directed ortho metalation. Tertiary amide and O-carbamate directors in synthetic strategies for polysubstituted aromatics. *Chem. Rev.* **90**, 879–933 (1990).
36. Knochel, P. & Cole, K. P. Directed ortho metalation in 2021: A tribute to Victor snieckus (August 1, 1937–december 18, 2020). *Org. Process Res. Dev.* **25**, 2188–2191 (2021).
37. Martínez-Martínez, A. J., Kennedy, A. R., Mulvey, R. E. & O'Hara, C. T. Directed ortho-meta'- and meta-meta'-dimetalations: A template base approach to deprotonation. *Science* **346**, 834–837 (2014).
38. Kuninobu, Y., Ida, H., Nishi, M. & Kanai, M. A meta-selective C–H borylation directed by a secondary interaction between ligand and substrate. *Nat. Chem.* **7**, 712–717 (2015).
39. Roque, J. B. et al. Kinetic and thermodynamic control of $C(sp^2)$–H activation enables site-selective borylation. *Science* **382**, 1165–1170 (2023).
40. Xue, C. et al. Ortho-Selective C–H Borylation of Aromatic Ethers with Pinacol-borane by organo rare-earth catalysts. *ACS Catal.* **8**, 5017–5022 (2018).
41. Su, X. et al. Nickel-catalyzed, silyl-directed, ortho-borylation of arenes via an unusual Ni(II)/Ni(IV) catalytic cycle. *Nat. Commun.* **15**, 7549 (2024).
42. Del Grosso, A., Singleton, P. J., Muryn, C. A. & Ingleson, M. J. Pinacol boronates by direct arene borylation with borenium cations. *Angew. Chem. Int. Ed.* **50**, 2102–2106 (2011).
43. Légaré, M.-A., Courtemanche, M.-A., Rochette, É & Fontaine, F.-G. Metal-free catalytic C-H bond activation and borylation of heteroarenes. *Science* **349**, 513–516 (2015).
44. Lv, J. et al. Metal-free directed sp^2-C–H borylation. *Nature* **575**, 336–340 (2019).
45. Furukawa, T., Tobisu, M. & Chatani, N. C. – H Functionalization at sterically congested positions by the platinum-catalyzed borylation of arenes. *J. Am. Chem. Soc.* **137**, 12211–12214 (2015).
46. Takeda, M., Nagao, K. & Ohmiya, H. Transition-metal-free cross-coupling by using tertiary benzylic organoboronates. *Angew. Chem. Int. Ed.* **59**, 22460–22464 (2020).
47. Katsoulos, G., Takagishi, S. & Schlosser, M. The Metalation of fluoroanisoles: Optional regioselectivity due to metal mediated control. *Synlett* **1991**, 731–732 (1991).
48. Schlosser, M. The 2×3 toolbox of organometallic methods for regiochemically exhaustive functionalization. *Angew. Chem. Int. Ed.* **44**, 376–393 (2005).
49. Whisler, M. C., MacNeil, S., Snieckus, V. & Beak, P. Beyond thermodynamic acidity: A perspective on the complex-induced proximity effect (CIPE) in deprotonation reactions. *Angew. Chem. Int. Ed.* **43**, 2206–2225 (2004).
50. Hayes, H. L. D. et al. Protodeboronation of (Hetero)arylboronic esters: Direct versus prehydrolytic pathways and self-/auto-catalysis. *J. Am. Chem. Soc.* **143**, 14814–14826 (2021).
51. Scott, K. A., Cox, P. B. & Njardarson, J. T. Phenols in pharmaceuticals: Analysis of a recurring motif. *J. Med. Chem.* **65**, 7044–7072 (2022).
52. Xie, B., Chen, Z., Ying, L., Huang, F. & Cao, Y. Near-infrared organic photoelectric materials for light-harvesting systems: Organic photovoltaics and organic photodiodes. *InfoMat* **2**, 57–91 (2020).
53. Unsinn, A. & Knochel, P. Regioselective zincation of indazoles using TMP2Zn and Negishi cross-coupling with aryl and heteroaryl iodides. *Chem. Commun.* **48**, 2680–2682 (2012).
54. Sandfort, F., Strieth-Kalthoff, F., Kühnemund, M., Beecks, C. & Glorius, F. A structure-based platform for predicting chemical reactivity. *Chem* **6**, 1379–1390 (2020).
55. Jorner, K., Tomberg, A., Bauer, C., Sköld, C. & Norrby, P.-O. Organic reactivity from mechanism to machine learning. *Nat. Rev. Chem.* **5**, 240–255 (2021).

56. Rinehart, N. I. et al. A machine-learning tool to predict substrate-adaptive conditions for Pd-catalyzed C–N couplings. *Science* **381**, 965–972 (2023).
57. Strieth-Kalthoff, F. et al. Machine learning for chemical reactivity: The importance of failed experiments. *Angew. Chem. Int. Ed.* **61**, e202204647 (2022).
58. Schleinitz, J. et al. Machine learning yield prediction from NiCOlit, a small-size literature data set of nickel catalyzed C–O couplings. *J. Am. Chem. Soc.* **144**, 14722–14730 (2022).
59. Segler, M. H. S., Preuss, M. & Waller, M. P. Planning chemical syntheses with deep neural networks and symbolic AI. *Nature* **555**, 604–610 (2018).
60. Brunel, J. M. BINOL: A versatile chiral reagent. *Chem. Rev.* **105**, 857–898 (2005).
61. Ma, L. et al. Synthesis and applications of 3-[6-(Hydroxymethyl) pyridin-2-yl]-1,1′-bi-2-naphthols or 3,3′-Bis[6-(hydroxymethyl)pyridin-2-yl]-1,1′-bi-2-naphthols. *Synthesis* **2007**, 2461–2470 (2007).
62. Jerca, F. A., Jerca, V. V. & Hoogenboom, R. Advances and opportunities in the exciting world of azobenzenes. *Nat. Rev. Chem.* **6**, 51–69 (2022).
63. Ishiyama, T., Murata, M. & Miyaura, N. Palladium(0)-catalyzed cross-coupling reaction of alkoxydiboron with haloarenes: A direct procedure for arylboronic esters. *J. Org. Chem.* **60**, 7508–7510 (1995).
64. Barroso, S. et al. Improvement in the Palladium-Catalyzed Miyaura Borylation Reaction by optimization of the base: scope and mechanistic study. *J. Org. Chem.* **86**, 103–109 (2021).
65. Lee, Y. et al. Chemoselective coupling of 1,1-Bis[(pinacolato)boryl] alkanes for the transition-metal-free borylation of aryl and vinyl halides: A combined experimental and theoretical investigation. *J. Am. Chem. Soc.* **139**, 976–984 (2017).

Acknowledgements

This work was supported by the National Natural Science Foundation of China (Nos. 22073043 from S.L., 22273035 from G. W.), and the National Key Research and Development Program of China (No. 2023YFB3813001, G.W.), the New Cornerstone Science Foundation (S.L.). We acknowledge the financial support by the Engineering Research Center of Photoresist Materials, Ministry of Education (G. W.). We thank Prof. Dr. Jing Ma and Prof. Dr. Jin Xie for their insightful discussions. We thank Mr. Changhui Dai for his help with polymer molecular weight measurements. We thank Mr. Yuhao Gu for his assistance with crystal structure determination. All theoretical calculations were performed at the High-Performance Computing Center (HPCC) of Nanjing University.

Author contributions

X.L., G.W. and S.L. conceived the work and designed the computational and experimental investigations. X.L. carried out most of the experiments with the help of M.W., S.Y., M.Y., S.C., Z.L., and L.G. X.L. also performed quantum-chemical calculations, with G.L. specifically assisting in the reaction network construction for key intermediate substrates. D.L. performed the machine learning model construction, with M.W. and L.H. assisting in dataset construction. X.L., G.W., and S.L. discussed the results and co-wrote the paper with the input from all the other authors. G.W. and S.L. supervised the project.

Competing interests

The authors declare no competing interests.

Additional information

Supplementary information The online version contains supplementary material available at https://doi.org/10.1038/s41467-025-60674-9.

Correspondence and requests for materials should be addressed to Guoqiang Wang or Shuhua Li.

Peer review information *Nature Communications* thanks Valerio Fasano and the other anonymous reviewer(s) for their contribution to the peer review of this work. A peer review file is available.